論文 / 著書情報
Article / Book Information

Title	Wideband design of a short-slot 2-plane coupler by the mode matching/FEM hybrid analysis considering the structural symmetry
Authors	Masahiro Wakasa, Dong-Hun Kim, Takashi Tomura, Jiro Hirokawa
Citation	IEICE TRANSACTIONS on Communications, vol. E102-B, no. 5, pp. 1019-1026
Pub. date	2019, 5
Copyright	Copyright (c) 2019 Institute of Electronics, Information and Communication Engineers.

PAPER

Wideband Design of a Short-Slot 2-Plane Coupler by the Mode Matching/FEM Hybrid Analysis Considering the Structural Symmetry

Masahiro WAKASA[†a)], **Dong-Hun KIM**[†], *Nonmembers*, **Takashi TOMURA**[†], *Member*, *and* **Jiro HIROKAWA**[†], *Fellow*

SUMMARY This paper presents the mode matching (MM)/finite element method (FEM) hybrid analysis for a short-slot 2-plane coupler, and an optimization process for a wideband design based on a genetic algorithm (GA). The method of the analysis combines a fast modal analysis of the MM which reduces the computation time, with the flexibility of an FEM which can be used with an arbitrary cross-section. In the analysis, the model is reduced into the one-eighth model by using the three-dimensional structural symmetry. The computed results agree well with those by the simulation and the computation time is reduced. The bandwidth is improved by the optimization based on the GA from 2.4% to 6.9% for the 2-plane hybrid coupler and from 5.4% to 7.5% for the 2-plane cross coupler. The measured results confirm the wideband design.

key words: *short-slot 2-plane coupler, mode matching technique, finite element method*

1. Introduction

In 1952, Riblet proposed the short-slot hybrid H-plane coupler [1], which gives an equally divided power and 90-degree phase difference between the two output ports. The short-slot coupler can also work as a cross coupler, which transfers input power towards the diagonal port of an input port, by doubling the length of the coupling region. The short-slot E-plane coupler works in the same manner as an H-plane coupler [2]. These short-slot couplers are used for components of several microwave circuits because of their high-power capability and low-loss operation in relation to use of hollow-waveguide structures.

The Butler matrix [3] is applied to beam-switching circuits. It can be applied by using short-slot hybrid and cross couplers and phase shifters, and enables one-dimensional beam-switching. However, if two-dimensional beam-switching is required, the short-slot H-plane and E-plane couplers have to be cascaded [4]. When the number of ports in the Butler matrix increases, more hybrid and cross couplers are required and its size rapidly increases. To overcome this problem, a short-slot 2-plane coupler has been proposed [5]. The proposed short-slot 2-plane coupler has a double layer structure with 4 input ports and 4 output ports. The functionality of the short-slot H-plane and E-plane coupler is combined into one body, and it works as a two-dimensional hybrid and cross coupler. With the short-slot 2-plane coupler the size of the Butler matrix can be made shorter than the cascade connection of H-plane and E-plane couplers. However, the bandwidth of the short-slot 2-plane coupler in [5] was narrow due to the difficulty of designing a large number of parameters. The report in [6] improved the bandwidth but still the bandwidth is still quite narrow.

In this paper, the short-slot 2-plane coupler is analyzed with a mode matching (MM)/finite element method (FEM) hybrid analysis [7] and optimized by a genetic algorithm [8]. The MM [9], [10] is appropriate for an analysis of a step discontinuous structure. Electric and magnetic fields in each region are expanded by their eigenmode functions. The expanded fields are applied to the boundary conditions on the discontinuous plane to match the fields, and this procedure leads to a generalized scattering matrix (GSM), which represents the reflection and transmission of each mode including evanescent modes. Since the MM requires only eigenmode functions in each region and only matrix calculations, it can provide a faster analysis. However, eigenmode functions must be known a priori, and the only analytical solutions of eigenmode functions are for canonical cross-sections. The MM/FEM hybrid analysis combines this fast analysis of the MM with the flexibility of the FEM which can be used to calculate the numerical solution of eigenmode functions for an arbitrary cross-section. This fast analysis enables optimizing of 13 parameters for the design of the short-slot 2-plane coupler by genetic algorithm (GA).

The main contribution of this paper is to present a wideband design of a short-slot 2-plane coupler by GA optimization. The paper is organized as follows. Section 2 describes the structure of the short-slot 2-plane coupler. In Sect. 3, the reduction of the region of the analysis and the theory and results of the analysis of the MM/FEM hybrid analysis are described. Section 4 shows the results of the optimized structure for the 2-plane hybrid and cross coupler. Section 5 demonstrates the measured results of the 2-plane hybrid. Finally, Sect. 6 summarizes the conclusions.

Manuscript received July 8, 2018.
Manuscript revised September 30, 2018.
Manuscript publicized October 23, 2018.

[†]The authors are with the Department of Electrical and Electronic Engineering, Tokyo Institute of Technology, Tokyo, 152-8552 Japan.
a) E-mail: wakasa.masahiro@jgc.com

DOI: 10.1587/transcom.2018EBP3202

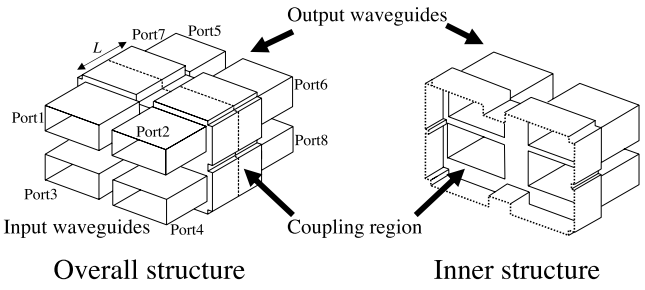

Fig. 1 Configuration of the short-slot 2-plane coupler.

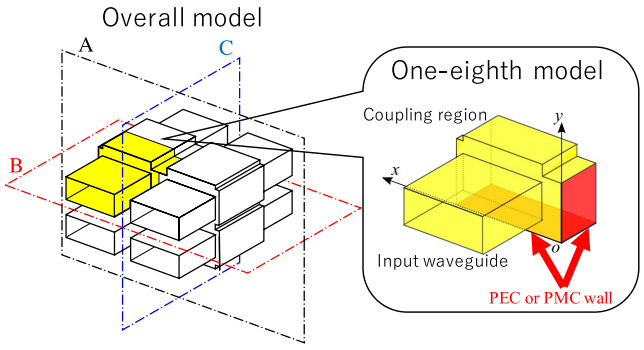

Fig. 2 Three-dimensional structural symmetry.

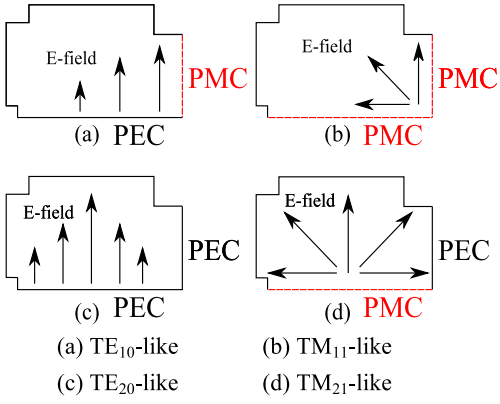

Fig. 3 Electromagnetic modes in the coupling region.

2. Configuration

The short-slot 2-plane coupler is shown in Fig. 1. The structure has 4 input waveguides and 4 output waveguides, and the coupling region. Incidence from one of the input waveguides for the 2-plane hybrid coupler gives equally divided power and a two-dimensional phase difference among the four output waveguides, and this function enables the two-dimensional beam-switching. The 2-plane cross coupler transfers the incident power to the diagonal output waveguide of the input waveguide. In order to achieve these functions, at least 4 types of electromagnetic modes are required in the coupling region.

3. Analysis Method

3.1 Reduction of the Analysis Region

The structure of the short-slot 2-plane coupler is symmetrical in the planes A, B and C as shown in Fig. 2. All of the electromagnetic modes in the coupling region can be expressed by the quarter region of the coupling region placed a PEC or PMC on each of the symmetrical planes B and C in consideration of the symmetry of the electromagnetic modes as shown in Fig. 3. With respect to the symmetrical plane A, the GSM of the full structure can be obtained by calculating a cascade connection of two of the GSM, reducing the structure of the to a one-eighth model.

3.2 Mode Matching/FEM Hybrid Analysis

The one-eighth model is analyzed by the MM/FEM hybrid analysis. The discontinuous plane formed by the input waveguides and the coupling region is assumed to be on the x-y plane as shown in Fig. 2. The analysis is conducted in the following 4 steps.

Step 1) Eigenmode expansion

The tangential components of the electric and magnetic fields both in the input region (Region I) and the coupling region (Region II) on the discontinuous plane are expanded with eigenmode functions by the following equations [11].

$$\boldsymbol{E}_t^{\mathrm{I}} = \sum_{i=1}^{N_{\mathrm{I}}} \left(a_i^{\mathrm{I}} + b_i^{\mathrm{I}}\right) \mathbf{e}_i^{\mathrm{I}}(x,y), \boldsymbol{H}_t^{\mathrm{I}} = \sum_{i=1}^{N_{\mathrm{I}}} \left(a_i^{\mathrm{I}} - b_i^{\mathrm{I}}\right) \mathbf{h}_i^{\mathrm{I}}(x,y) \quad (1)$$

$$\boldsymbol{E}_t^{\mathrm{II}} = \sum_{i=1}^{N_{\mathrm{II}}} \left(b_i^{\mathrm{II}} + a_i^{\mathrm{II}}\right) \mathbf{e}_i^{\mathrm{II}}(x,y), \boldsymbol{H}_t^{\mathrm{II}} = \sum_{i=1}^{N_{\mathrm{II}}} \left(b_i^{\mathrm{II}} - a_i^{\mathrm{II}}\right) \mathbf{h}_i^{\mathrm{II}}(x,y) \quad (2)$$

where a_i^p, b_i^p $(p = \mathrm{I}, \mathrm{II})$ are the expansion coefficients of the fields in region p, which propagate from the discontinuous plane and towards the discontinuous plane respectively, and $\mathbf{e}_i^p(x,y), \mathbf{h}_i^p(x,y)$ are the eigenmode functions of the electric and magnetic fields in the region p respectively. Since the input waveguide has a rectangular cross-section, the eigenmode functions can be obtained analytically. However, the eigenmode functions in the coupling region cannot be obtained analytically. Therefore, the eigenmode functions for the cross-section of the coupling region are calculated numerically with the two-dimensional FEM. The cross-section of the coupling region is discretized with first-order rectangular vector basis functions. Here, the eigenmode functions in each region are normalized by the following expression in order to orthonormalize them.

$$\int_{S_p} \mathbf{e}_i^p(x,y) \times \mathbf{h}_i^p(x,y) \cdot \hat{z} dS = \delta_{ij} \quad (3)$$

where $S_p (p = \mathrm{I}, \mathrm{II})$ are the cross-section of each region and δ_{mn} is the Kronecker delta. The area of S_{II} is larger than that of S_{I}.

Step 2) Applying Galerkin's method

Simultaneous integral equations are derived by applying Galerkin's method to the continuity conditions of the

tangential components of the electric and magnetic fields on the discontinuous plane. The continuity conditions where the input waveguide is completely included in the coupling region (Fig. 4(a)), and where the input waveguide is not completely included in the coupling region (Fig. 4(b)) can be expressed as follows [11].

$$\begin{aligned} \boldsymbol{E}_t^{\mathrm{II}} &= \begin{cases} \boldsymbol{0} & \text{in } S_c \\ \boldsymbol{E}_t^{\mathrm{I}} & \text{in } S_m \end{cases} \\ \boldsymbol{H}_t^{\mathrm{I}} &= \boldsymbol{H}_t^{\mathrm{II}} \quad \text{in } S_m \end{aligned} \qquad \text{for } S_m = S_{\mathrm{I}} \tag{4}$$

$$\begin{aligned} \boldsymbol{E}_t^{p} &= \begin{cases} \boldsymbol{0} & \text{in } S_c \\ \boldsymbol{E}_t^{m} & \text{in } S_m \end{cases} \quad (p = \mathrm{I}, \mathrm{II}) \\ \boldsymbol{H}_t^{\mathrm{I}} &= \boldsymbol{H}_t^{\mathrm{II}} \quad \text{in } S_m \end{aligned} \qquad \text{for } S_m \neq S_{\mathrm{I}} \tag{5}$$

where $S_m = S_{\mathrm{I}} \cap S_{\mathrm{II}}$, $S_c = S_{\mathrm{I}} \cup S_{\mathrm{II}} - S_m$, and $\boldsymbol{E}_t^m$ is the tangential components of the electric fields on the plane S_m and expressed as follows using eigemode functions $\mathbf{e}_i^m(x, y)$ and the expansion coefficient c_i.

$$\boldsymbol{E}_t^m = \sum_{i=1}^{N_m} c_i \mathbf{e}_i^m(x, y) \tag{6}$$

Then, by taking cross products of Eqs. (4)–(5) and magnetic (electric) basis functions, and integrating over the cross-section S_{II} (S_{I}) for the continuity conditions of the electric (magnetic), the following simultaneous integral equations can be obtained.

$$\begin{aligned} \mathbf{X}^t (\boldsymbol{a}_{\mathrm{I}} + \boldsymbol{b}_{\mathrm{I}}) &= (\boldsymbol{a}_{\mathrm{II}} + \boldsymbol{b}_{\mathrm{II}}) \\ (\boldsymbol{b}_{\mathrm{I}} - \boldsymbol{a}_{\mathrm{I}}) &= \mathbf{X} (\boldsymbol{a}_{\mathrm{II}} - \boldsymbol{b}_{\mathrm{II}}) \end{aligned} \qquad \text{for } S_m = S_{\mathrm{I}} \tag{7}$$

$$\begin{aligned} (\boldsymbol{a}_{\mathrm{I}} + \boldsymbol{b}_{\mathrm{I}}) &= \mathbf{Y}_{\mathrm{I}}^t \boldsymbol{c}, (\boldsymbol{a}_{\mathrm{II}} + \boldsymbol{b}_{\mathrm{II}}) = \mathbf{Y}_{\mathrm{II}}^t \boldsymbol{c} \\ \mathbf{Y}_{\mathrm{II}} (\boldsymbol{a}_{\mathrm{II}} - \boldsymbol{b}_{\mathrm{II}}) &= \mathbf{Y}_{\mathrm{I}} (\boldsymbol{b}_{\mathrm{I}} - \boldsymbol{a}_{\mathrm{I}}) \end{aligned} \qquad \text{for } S_m \neq S_{\mathrm{I}} \tag{8}$$

where $\boldsymbol{a}_p, \boldsymbol{b}_p (p = \mathrm{I}, \mathrm{II})$ and $\boldsymbol{c}$ are vectors, whose elements are a_n^p, b_n^p and c_n respectively. The $\mathbf{X}$ and $\mathbf{Y}_p (p = \mathrm{I}, \mathrm{II})$ are coupling matrices, which represent the mode coupling between the regions, and is expressed as follows [11].

$$[X]_{ij} = \int_{S_m} \mathbf{e}_i^{\mathrm{I}}(x, y) \times \mathbf{h}_j^{\mathrm{II}}(x, y) \cdot \hat{z} dS \tag{9}$$

$$\left[Y_p\right]_{ij} = \int_{S_m} \mathbf{e}_i^m(x, y) \times \mathbf{h}_j^p(x, y) \cdot \hat{z} dS \quad (p = \mathrm{I}, \mathrm{II}) \tag{10}$$

Step 3) Calculation of the coupling matrix

The integrand in Eqs. (9) and (10) is a cross product of a trigonometric function and the first-order vector basis function or two first-order vector basis functions. Therefore, the integrand can be calculated analytically, and no numerical integration is required. The elements of the coupling matrix can be divided into a frequency dependent factor, which consists of the impedance of each eigenmode, and a frequency independent factor, to save calculation time for a frequency sweep. In addition, for the case where the area of S_p is fully included in the area of S_q, the TE modes in region q and TM modes in region p do not couple with each other [12], and the integrals in Eqs. (9) and (10) are always zero.

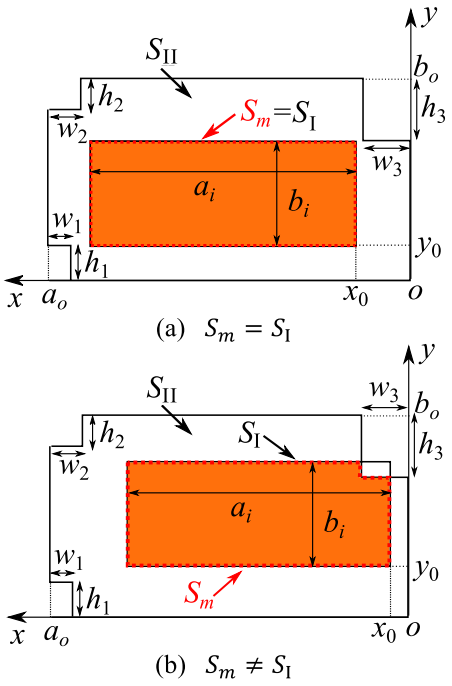

Fig. 4 Cross section of the structure on the discontinuous plane.

Step 4) Calculation of the GSM

By solving the simultaneous Eqs. (7) and (8) using the obtained coupling matrices, the GSM of the one-eighth model can be obtained.

3.3 Full Model Analysis

The GSM of the overall structure is calculated by using the obtained GSM of the one-eighth model and the structural symmetry. With respect to the symmetrical plane A, the GSM of the quarter model, which includes the input and output waveguides, is obtained by calculating a cascade connection of the GSM [13] of the one-eighth model. With respect to the symmetrical planes B and C, taking the polarity of the electric fields of each mode at the position of the input waveguide into consideration, the GSM of the overall structure is derived by adding or subtracting the GSM of the quarter model for the four cases shown in Fig. 3 as follows.

$$\begin{aligned} S_{51[11]} &= \frac{1}{4}\left(S^a_{21[11]} + S^b_{21[11]} + S^c_{21[11]} + S^d_{21[11]}\right) \\ S_{61[21]} &= \frac{1}{4}\left(S^a_{21[11]} + S^b_{21[11]} - S^c_{21[11]} - S^d_{21[11]}\right) \\ S_{71[31]} &= \frac{1}{4}\left(S^a_{21[11]} - S^b_{21[11]} + S^c_{21[11]} - S^d_{21[11]}\right) \\ S_{81[41]} &= \frac{1}{4}\left(S^a_{21[11]} - S^b_{21[11]} - S^c_{21[11]} + S^d_{21[11]}\right) \end{aligned} \tag{11}$$

where $S^r_{21[11]} (r = a, b, c, d)$ are S-parameters S_{21} and S_{11} of the quarter model for the four cases shown in Fig. 3(a)–(d). The GSM for an excitation to other input ports can also be obtained in the same way.

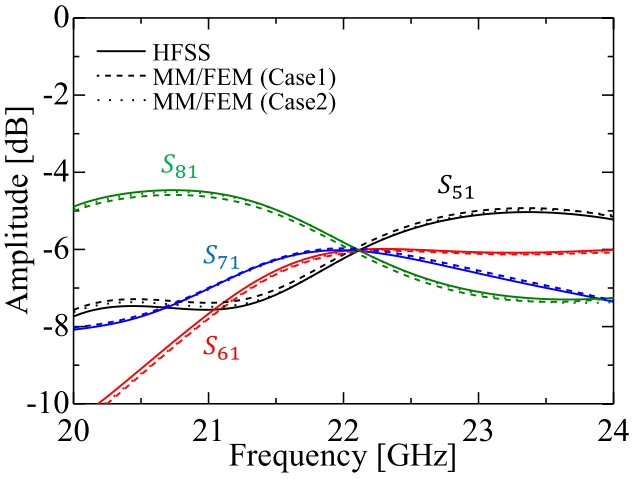

Fig. 5 Amplitude in the 2-plane hybrid coupler.

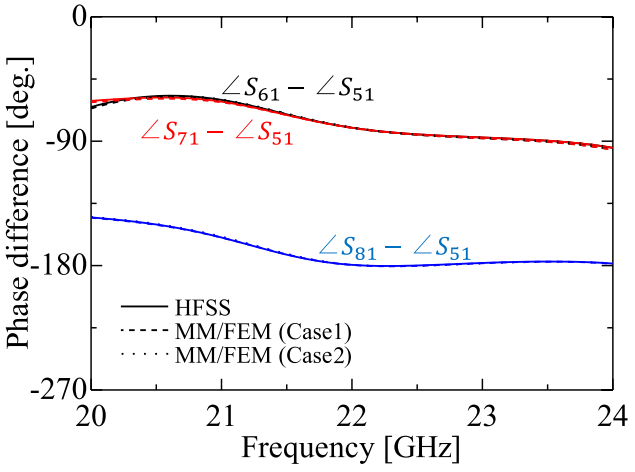

Fig. 6 Phase differences in the 2-plane hybrid coupler.

3.4 Analysis Results

The results of the analysis method mentioned above are discussed in this section. The parameters of the model are the conventionally designed 2-plane hybrid coupler [5] for the 22 GHz band.

The computed S-parameters of the output waveguides when an input signal is excited from the input waveguide 1 are shown in Fig. 5 with the results by the simulation software HFSS. The phase differences between two of the output waveguides are also shown in Fig. 6. In the MM/FEM hybrid analysis, there are two factors to consider about analysis accuracy [14]. The first is convergence of numerical solutions of eigenmode functions in the coupling region by FEM. The second consideration is the number of electromagnetic modes considered in the calculation of the coupling matrices. In the mode matching technique, it is known that the GSM converges to an erroneous value if the number of electromagnetic modes considered in each region is not selected properly [15]–[17]. In this paper, the number

Table 1 Calculation conditions.

		Case 1	Case 2
Number of basis functions	Coupling region	34776	4634
	Cross-section S_m	21480	2773
Maximum cutoff wavenumber [1/m]		4000	2700
Number of modes	Input waveguide	TE(50)TM(36)	TE(24)TM(15)
	Cross-section Sm	TE(51)TM(36)	TE(23)TM(14)
	Coupling region-a	TE(77)TM(62)	TE(37)TM(27)
	Coupling region-b	TE(73)TM(71)	TE(32)TM(31)
	Coupling region-c	TE(79)TM(59)	TE(38)TM(26)
	Coupling region-d	TE(74)TM(66)	TE(34)TM(29)

of the electromagnetic modes in each region N_{I}, N_{II} and N_m are determined so that the maximum cutoff wavenumber $k_{c\max}$ of the electromagnetic modes considered are same in each region. In order to confirm the convergence of the method mentioned above, the analysis was conducted under two conditions listed in Table 1. The four types of the coupling regions in Table 1 correspond to those in Fig. 3. Even the results for the Case 2 agree well with those by the HFSS.

The computation times for the derivation of all eigenmode functions in the four cases shown in Fig. 3 are 68.2 and 4.7 seconds for the Cases 1 and 2 respectively, and 71.6 and 2.0 seconds for the calculation of the GSM of the whole structure at 100 frequency points using a computer with Intel Core i7 CPU with 3.4 GHz and 16-GB memory. Note that eigenmode functions are derived only once since the eigenmode functions do not depend on the frequency. For the analysis by the HFSS, the overall structure is modeled and discretized with the three-dimensional FEM and the computation time is 204 seconds.

4. Wideband Design by Genetic Algorithm

The 2-plane hybrid and cross couplers are designed to widen the bandwidth by combining the Genetic Algorithm (GA) and the MM/FEM hybrid analysis. By optimizing 13 parameters using the MATLAB function “ga” [18], which includes 12 parameters on the cross-section of the structure shown in Fig. 4 and the length of the coupling region l, the bandwidth of the structure is improved. The key issues to widen the bandwidth are to divide the input power equally among the four types of electromagnetic modes shown in Fig. 3, and reduce the frequency fluctuation of these characteristics. Optimizing a large number of parameters with a commercial simulation software is not practical because of the computation time required. The MM/FEM hybrid analysis mentioned in the previous section provides a faster calculation and enables the design with 13 parameters.

For the GA process, parameter values are encoded into binary strings, and the fitness function $f = BW$ is evaluated using the GSM calculated by the MM/FEM hybrid analysis,

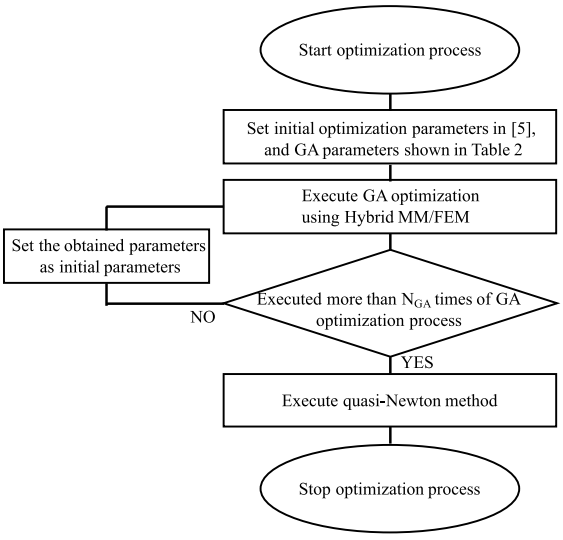

Fig. 7 Design flow chart.

Table 2 GA parameters.

Number of opt. parameters	13
Population per generation	40
Number of generation	30
Number of elites	2
Selection algorithm	Stochastic universal sampling
Mutation algorithm	Adaptive mutation
Crossover algorithm	Intermediate crossover
Crossover rate	0.7

where BW is the bandwidth in which the following conditions are satisfied.

For the 2-plane hybrid coupler

- $|S_{51}|$, $|S_{61}|$, $|S_{71}|$ and $|S_{81}|$ are within -6.02 ± 0.5 [dB]
- $\angle S_{61} - \angle S_{51}$, $\angle S_{71} - \angle S_{51}$ are within 90 ± 10 [deg.]
- $\angle S_{81} - \angle S_{51}$ is within 180 ± 10 [deg.]

For the 2-plane cross coupler

- $|S_{81}| \geq -0.5$ [dB]

The fitness function is defined as the bandwidth itself where the above conditions are satisfied. The bandwidth for a 2-plane hybrid coupler corresponds to a degradation of directivity of the 4-array aperture by 0.24 dB compared to the ideal value at the center frequency. The design flow chart is shown in Fig. 7 and the parameters used for the GA optimization are listed in Table 2. The design parameters in the conventional study [5], where the bandwidth is 2.4% and 5.4% for the 2-plane hybrid and cross couplers, respectively, are used as initial values for the GA optimization. In [5], the short-slot 2-plane coupler was designed by tuning 13 parameters manually. The optimized parameters are listed in Table 3. Figures 8 and 9 represent the improved frequency characteristics of the 2-plane hybrid coupler, and

Table 3 Optimized parameters [mm].

2-plane Hybrid coupler

a_i	8.08	h_1	0.40
b_i	4.24	w_2	1.12
a_o	10.3	h_2	1.28
b_o	6.56	w_3	1.76
x_0	0.60	h_3	1.76
y_0	0.68	l	13.2
w_1	0.72		

2-plane Cross coupler

a_i	8.21	h_1	0.49
b_i	4.68	w_2	1.92
a_o	10.4	h_2	1.73
b_o	6.95	w_3	1.52
x_0	0.40	h_3	2.04
y_0	0.84	l	26.9
w_1	1.36		

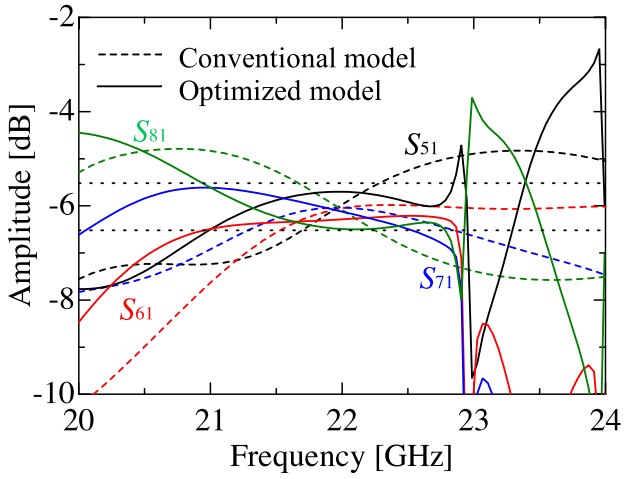

Fig. 8 Amplitude in the optimized 2-plane hybrid coupler compared to the conventional model.

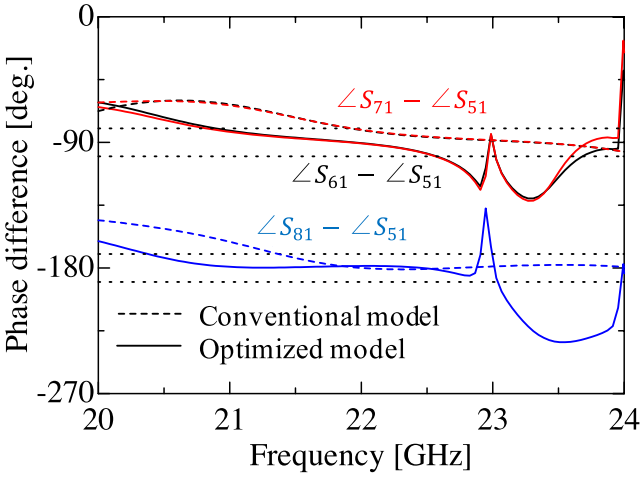

Fig. 9 Phase differences in the optimized 2-plane hybrid coupler compared to the conventional model.

our results are comparable to those in [5]. The dashed horizontal lines show the ranges where the conditions mentioned above are satisfied. The optimized results show that the improved performance, and the bandwidth is improved from 2.4% to 6.9%. Fig. 10 shows electromagnetic modes in the coupling region classified into the four types shown

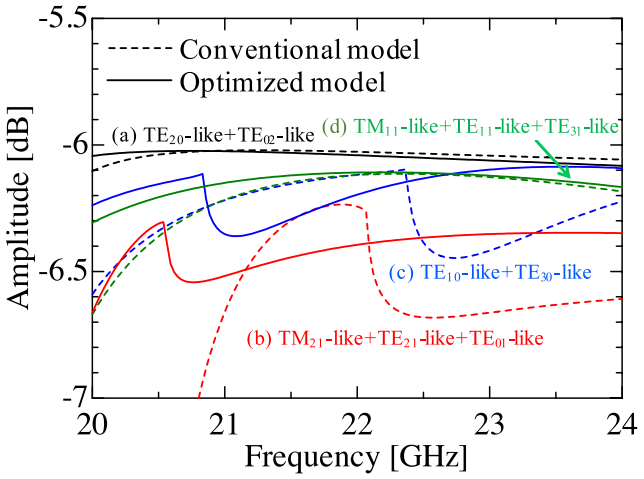

Fig. 10 Coupling coefficients of electromagnetic modes between the input waveguide and the coupling region for the 2-plane hybrid coupler.

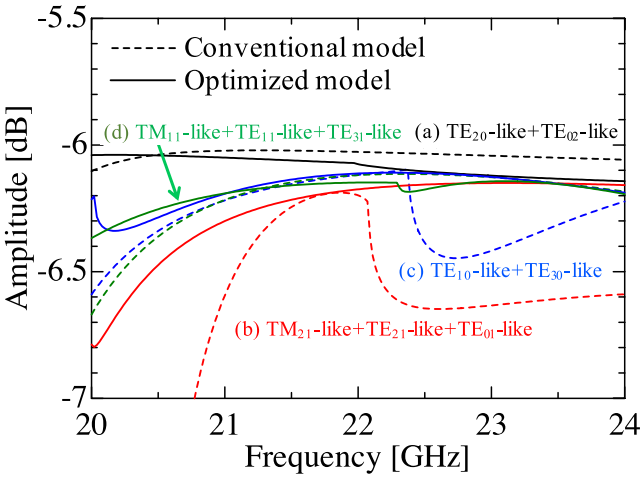

Fig. 12 Coupling coefficients of electromagnetic modes between the input waveguide and the coupling region for the 2-plane cross coupler.

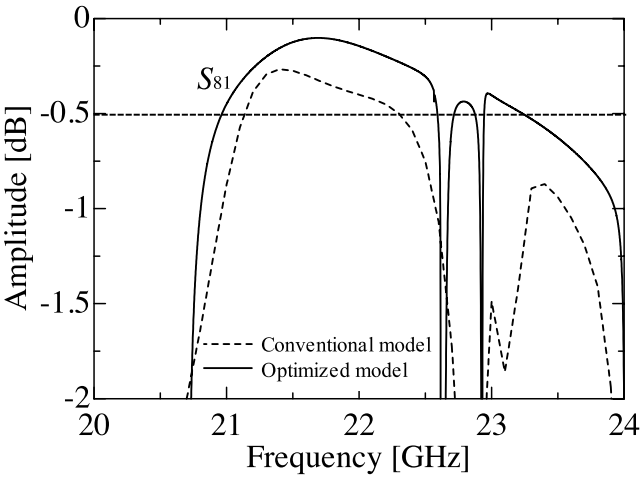

Fig. 11 Amplitude in the optimized 2-plane cross coupler compared to the conventional model.

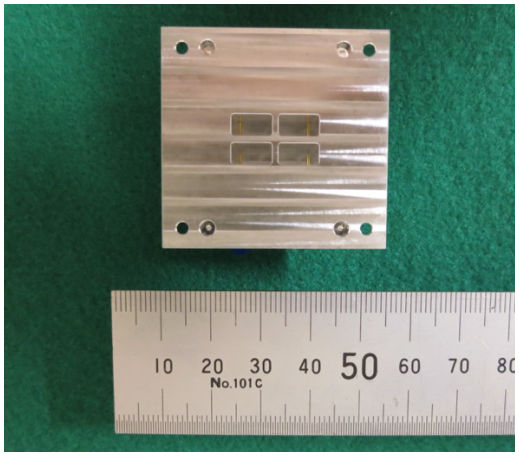

Fig. 13 Fabricated short-slot 2-plane coupler.

in Fig. 3 according to the polarity of the electric fields. The results in Figs. 10 and 11 with four colors correspond to the GSM of the four types of one-eighth models by multiplying each amplitude by 4. In the design of the conventional study, only four electromagnetic modes (TE_{10}-like, TE_{11}-like, TE_{20}-like, and TM_{21}-like) are considered, and the frequency characteristics of those modes have narrow bandwidths in terms of flatness. In the design of the optimized model, additional six electromagnetic modes (TE_{01}-like, TM_{11}-like, TE_{02}-like, TE_{21}-like TE_{30}-like, and TE_{31}-like) are considered, to compensate for the fluctuations in the frequency characteristics.

The results of the 2-plane cross coupler are also shown in Fig. 10 together with those of the conventional model. The bandwidth is improved from 5.4% to 7.5% by making use of additional electromagnetic modes as shown in Fig. 11. In the results of the optimized models, the frequency characteristics have several sharp dips because of resonance phenomena in the coupling region. In the design, those resonant frequencies are avoided for the desired bandwidth.

5. Experimental Results

An optimized short-slot 2-plane hybrid coupler is fabricated and shown in Fig. 13. The measurements are carried out with a VNA, and coaxials to waveguide transitions are used for the measurement. The measurement results are shown in Fig. 14 and Fig. 15. The solid lines show the measurement results and the dashed lines show the results of the simulation. The effects of the transitions are eliminated by calibration. The results agree well with those obtained by the simulation. In the range of the designed bandwidth of 6.9%, the measurement results of the output amplitude are within -6.02 ± 1.12 [dB], and those of the phase differences among the output ports are -90.0 ± 12.5 [deg.] for $\angle S_{61} - \angle S_{51}$ and $\angle S_{71} - \angle S_{51}$, and -180.0 ± 5.52 [deg.] for $\angle S_{81} - \angle S_{51}$.

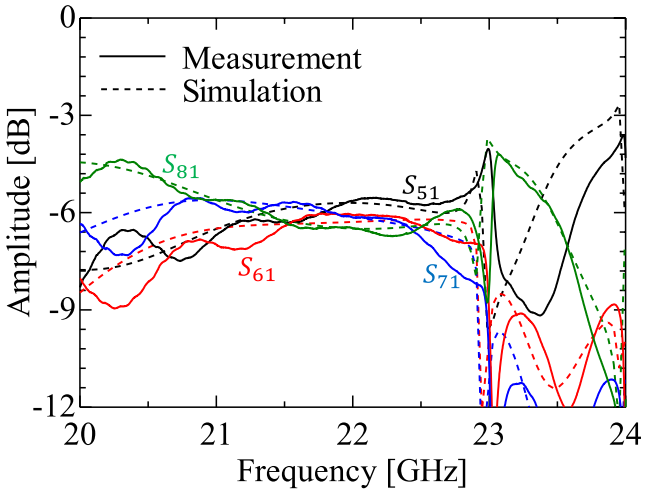

Fig. 14 Measurement results of the output amplitude for the optimized 2-plane hybrid coupler.

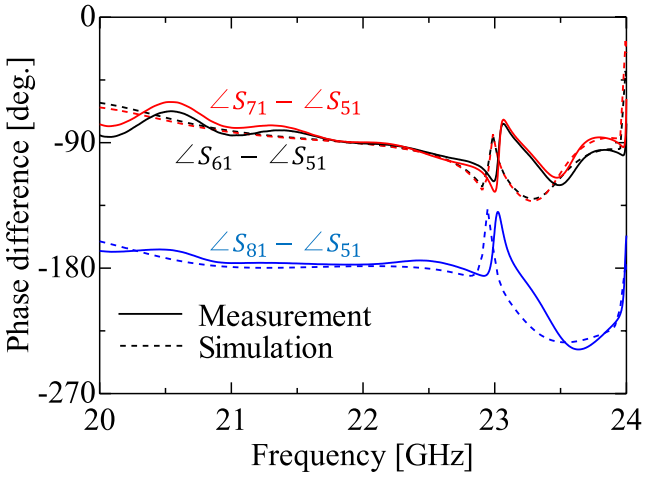

Fig. 15 Measurement results of the phase differences among the output ports for the optimized 2-plane hybrid coupler.

6. Conclusions

A wideband short-slot 2-plane coupler is designed and fabricated. For the design, the structure is analyzed with mode matching/FEM hybrid analysis, and the computation time is reduced from 204 seconds by the HFSS to 6.7 seconds by the proposed method. The bandwidth is improved by the optimization based on the GA from 2.4% to 6.9% for the 2-plane hybrid coupler and from 5.4% to 7.5% for the 2-plane cross coupler. Also, the measurement results of the 2-plane hybrid coupler agree well with the simulation results.

Acknowledgments

This work is conducted in part by the Strategic Information and Communications R&D Promotion Programme (185004002), the Ministry of Internal Affairs and Communications.

References

[1] H.J. Riblet, "The short-slot hybrid junction," Proc. IRE, vol.40, pp.180–184, Feb. 1952.
[2] J.A. Ruiz-Cruz, J.R. Montejo-Garai, and J.M. Rebollar, "Short-slot E-plane and H-plane waveguide couplers with an arbitrary power division ratio," Intl. J. Electron., vol.98, no.1, pp.11–24, 2011.
[3] J. Butler and R. Lowe, "Beam forming matrix simplifies design of electronically scanned antennas," Electron. Design, vol.9, pp.170–173, April 1961.
[4] B. Pattan, "The versatile butler matrix," Microw. J., vol.47, no.11, pp.126–138, 2004.
[5] D.H. Kim, J. Hirokawa, and M. Ando, "Design of waveguide short-slot two-plane couplers or one-body 2-D beam-switching butler matrix application," IEEE Trans. Microw. Theory Techn., vol.64, no.3, pp.776–784, March 2016.
[6] D.H. Kim, J. Hirokawa, and M. Ando, "Wideband waveguide short-slot 2-plane coupler using frequency shift of propagating modes," IEICE Trans. Electron., vol.E101-C, no.10, pp.815–821, Oct. 2018.
[7] D. Arena, M. Ludovico, G. Manara, and A. Monorchio, "A hybrid mode matching/FEM technique with edge elements for solving waveguides discontinuity problems," IEEE AP-SInt. Symp. Dig., vol.4, pp.2028–2031, July 2000.
[8] J. Holland, Adaptation in Natural and Artificial Systems, The university of Michigan, 1975.
[9] A. Wexler, "Solution of waveguide discontinuities by modal analysis," IEEE Trans. Microw. Theory Techn., vol.MTT-15, no.9, pp.508–517, Sept. 1967.
[10] P.H. Masterman and P.J.B. Clarricoats, "Computer field-matching solution of waveguide transverse discontinuities," Proc. Inst. Elec. Eng., vol.118, no.1, pp.51–63, Jan. 1971.
[11] V. Zhurbenko, Passive Microwave Components and Antennas, ch.6, InTech, 2012.
[12] G.G. Gentili, "Properties of TE/TM mode matching techniques," IEEE Trans. Microw. Theory Techn., vol.39, no.9, pp.1669–1673, Sept. 1991.
[13] D. Budimir, Generalized Filter Design by Computer Optimization, 1st ed., Appendix.A, Artech House Publishers, 1998.
[14] D. Arena, M. Ludovico, G. Manara, and A. Monorchio, "Analysis of waveguide discon-tinuities using edge element in a hybrid mode matching/finite elements approach," IEEE Microw. Compon. Lett., vol.11, no.9, pp.379–381, Sept. 2001.
[15] R. Mittra, "Relative convergence of the solution of a doubly infinite set of equations," J. Res. Nat. Bur. Stand., vol.67D, no.2, pp.245–254, March-April 1963.
[16] S.W. Lee, W.R. Jones, and J.J. Campbell, "Convergence of numerical solutions of Iris-type waveguide discontinuity problems," IEEE Trans. Microw. Theory Techn., vol.MTT-19, pp.528–536, June 1971.
[17] M. Leroy, "On the convergence of numerical results in modal analysis," IEEE Trans. Antennas Propag., vol.31, no.7, pp.655–659, July 1983.
[18] The MathWorks, Inc. "Genetic Algorithm," http://www.mathworks.com/discovery/genetic-algorithm.html

Masahiro Wakasa was born in Akita, Japan. He received the B.S. and M.S. degrees in Electrical and Electronic Engineering from the Tokyo Institute of Technology in 2015 and 2018, respectively. He joined JGC corporation in 2018, where he was engaged in plant system designs.

Dong-Hun Kim was born in Busan, Korea, on February 25, 1983. He received the B.S. degree in electrical and electronic engineering from the Yonsei University, Seoul, Korea, in 2008, the M.S. degree in environmental studies from the Tohoku University, Sendai, Japan, in 2011, and D.E. degrees in electrical and electronic engineering from the Tokyo Institute of Technology (Tokyo Tech), Tokyo, Japan in 2017. From 2011 to 2014, he worked at the Materials & Components R&D Lab., LG Electronics, and was engaged in the research of plasma diagnosis and the development of matching network for Plasma Lighting System. Since 2017, he has been with the SEMES Co. Ltd, Hwaseong, Korea, where he is currently a senior engineer. His current research interests include microwave and RF in the semiconductor equipment.

Takashi Tomura was born in Sendai, Japan. He received the B.S., M.S. and D.E. degrees in electrical and electronic engineering from the Tokyo Institute of Technology, Tokyo, Japan, in 2008, 2011 and 2014, respectively. He was a Research Fellow of the Japan Society for the Promotion of Science (JSPS) in 2013. From 2014 to 2017, he worked at Mitsubishi Electric Corporation, Tokyo and was engaged in research and development of aperture antennas for satellite communications and radar systems. He is currently a Specially Appointed Assistant Professor at the Tokyo Institute of Technology, Tokyo. His research interests include electromagnetic analysis, aperture antennas and planar waveguide slot array antennas. Dr. Tomura received the Best Student Award from Ericsson Japan in 2012 and the IEEE AP-S Tokyo Chapter Young Engineer Award in 2015. He is a member of the IEICE.

Jiro Hirokawa received the B.S., M.S. and D.E. degrees in electrical and electronic engineering from Tokyo Institute of Technology (Tokyo Tech), Tokyo, Japan in 1988, 1990 and 1994, respectively. He was a Research Associate from 1990 to 1996 and an Associate Professor from 1996 to 2015 at Tokyo Tech. He is currently a Professor there. He was with the antenna group of Chalmers University of Technology, Gothenburg, Sweden, as a Postdoctoral Fellow from 1994 to 1995. His research area has been in slotted waveguide array antennas and millimeter-wave antennas. He received IEEE AP-S Tokyo Chapter Young Engineer Award in 1991, Young Engineer Award from IEICE in 1996, Tokyo Tech Award for Challenging Research in 2003, Young Scientists' Prize from the Minister of Education, Cultures, Sports, Science and Technology in Japan in 2005, Best Paper Award in 2007 and a Best Letter Award in 2009 from IEICE Communications Society, and IEICE Best Paper Award in 2016. He is a Fellow of IEEE and IEICE.